Magnetic Currents Representing Magnetomotive Force for Magnetic Field Computation

Hisashi Endo[1], *Member, IEEE*, Toshiyuki Takagi[1], *Member, IEEE*, and Yoshifuru Saito[2], *Member, IEEE*

[1]Institute of Fluid Science, Tohoku University, Sendai 980-8577, Japan
[2]Graduate School of Engineering, Hosei University, Tokyo 184-8584, Japan

This paper proposes a formulation for magnetomotive force (MMF) employing the magnetic currents. Our formulation introduces the classical MMF into the modern magnetic field computation. The rotation of electric field represents the external magnetic field due to impressed voltage. We demonstrate a magnetic field computation of toroidal inductors by finite elements. Comparison with the computed result using the Biot-Savart law verifies our formulation. It is also verified by the experiments on the air- and magnet-core inductors.

Index Terms—**Linearized Chua-type magnetization model, magnetic currents, magnetic field computation, magnetomotive force.**

I. Introduction

THE CONCEPT of magnetomotive force (MMF) has been widely used to analyze the magnetic devices by means of the classical magnetic circuits [1]–[3]. It is obvious that modern computational methodologies are required to treat complicated structures for up-to-date devices. However, it has been difficult to introduce MMF into the integral and partial differential equations in the magnetic field computation [4]. The study behind this background is motivated to introduce MMF into the modern magnetic field computation. Thereby, we propose a formulation employing magnetic currents [5].

Our formulation for magnetic field computation is that the equivalent magnetic field source is derived in terms of the electric polarization, namely, magnetic currents [5]–[7]. In this case, it enables us voltage source computation. Stokes's theorem shows that the magnetic current is closely related with MMF. Therefore, it is possible to convert an electric current into a magnetic current as an equivalent magnetic field source in the orthogonal direction.

To demonstrate the validity of our formulation, the present paper computes the magnetic fields of toroidal inductors by means of finite elements taking unbounded effects [8], [9] and magnetic hysteresis [10], [11] into account. An analytical approach by Biot–Savart law and the experiments for an air-core inductor verify our formulation in terms of field distribution. Furthermore, the measured hysteretic loop of magnetic-core inductor is well reproduced by computation employing a linearized Chua-type magnetization model.

II. Representation of MMF by Magnetic Currents

A. Magnetic Currents

We consider the equivalent representation of MMF as the orthogonal component of the exciting current as shown in Fig. 1. Namely, the rotation of electric field $\mathbf{E}$ (V/m) is introduced as

$$\nabla \times \mathbf{D} = \nabla \times (\varepsilon_0 \mathbf{E} + \mathbf{P})$$

or

$$\nabla \times \mathbf{E} = \mathbf{J}_m - \frac{\partial \mathbf{B}}{\partial t} \tag{1}$$

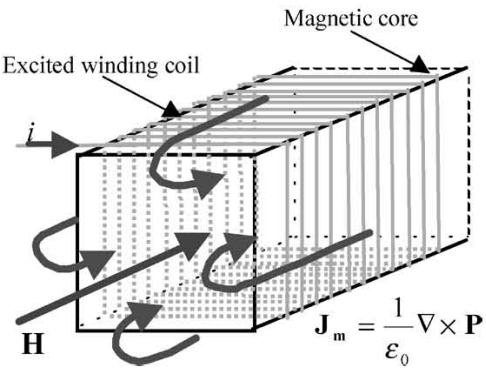

Fig. 1. Relation between the magnetomotive force and magnetic currents.

where $\mathbf{D}$ (C/m^2), ε_0 (F/m), $\mathbf{P}$ (C/m^2), and $\mathbf{J}_m$ (V/m^2) respectively denote the electric flux density, permittivity in vacuum, polarization, and magnetic current density given by

$$\mathbf{J}_m = \frac{1}{\varepsilon_0} \nabla \times \mathbf{P}. \tag{2}$$

Apply the surface integral to (1), then the line integral along with the winding coil path l can be derived from Stokes's theorem

$$\frac{1}{\varepsilon_0} \int \nabla \times \mathbf{D}\, d\mathbf{s} = \frac{1}{\varepsilon_0} \int \nabla \times \mathbf{P}\, d\mathbf{s} - \int \frac{\partial \mathbf{B}}{\partial t}\, d\mathbf{s} \tag{3}$$

$$\int \mathbf{E}\, d\mathbf{l} = \frac{1}{\varepsilon_0} \int \mathbf{P}\, d\mathbf{l} - \int \frac{\partial \mathbf{B}}{\partial t}\, d\mathbf{s}. \tag{4}$$

Since the first term on the right-hand side of (4) has the dimension of voltage, then the magnetic current density $\mathbf{J}_m$ corresponds to voltage per unit area caused by magnetic charge moving. Thus, $\mathbf{J}_m$ times conductivity σ (S/m) of the coil material is equivalent to MMF generating in volume surrounded by the exciting coils.

B. Continuity

In order to derive governing equations based on partial differential equations, we have to review the nature of magnetic currents. Maxwell equations concerning electric fields can be expressed as

$$\nabla \times \mathbf{E} = \mathbf{J}_m \quad \text{in static field} \tag{5}$$

$$\nabla \times \mathbf{E} = \mathbf{J}_m - \frac{\partial \mathbf{B}}{\partial t} \quad \text{in quasi-static dynamic field} \tag{6}$$

Digital Object Identifier 10.1109/TMAG.2005.845063

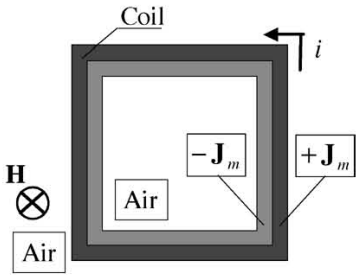

Fig. 2. Magnetic currents for the field of one turn coil.

where $\mathbf{B}$ (T) denotes the magnetic flux density. The divergences of both sides of (5) and (6) mathematically reduce to zero. In case of (6), the following condition should be satisfied:

$$\nabla \bullet \mathbf{J}_m = \nabla \bullet \frac{\partial \mathbf{B}}{\partial t}. \tag{7}$$

Since $\mathbf{J}_m$ is defined by the rotation of polarization $\mathbf{P}$, then the divergence of $\mathbf{J}_m$ is identical to zero [4]

$$\nabla \bullet \mathbf{J}_m = \nabla \bullet \frac{1}{\varepsilon_0} \nabla \times \mathbf{P} = 0. \tag{8}$$

Thus, the continuity of magnetic flux, expressed in (9), is independently satisfied

$$\nabla \bullet \mathbf{B} = 0. \tag{9}$$

Because of (9), most of the magnetic field computation methodologies have been employing the magnetic vector potential $\mathbf{A}$ (Wb/m).

C. Governing Equations for Magnetic Fields

Let us consider the magnetic field of one turn coil shown in Fig. 2. Impose (9), then the governing equations in terms of the magnetic field $\mathbf{H}$ (A/m) result in

$$\nabla^2 \mathbf{H} = -\sigma \mathbf{J}_m \quad \text{in static field} \tag{10}$$

$$\nabla^2 \mathbf{H} - \sigma\mu \frac{d\mathbf{H}}{\partial t} = -\sigma \mathbf{J}_m \quad \text{in quasi-static field} \tag{11}$$

where μ (H/m) is the permeability. Since $\mathbf{J}_m$ gives voltage per unit area, then $-\sigma \mathbf{J}_m$ in the right sides of (10) and (11) is related with the exciting electric current i (A). Moreover, $\mathbf{J}_m$ is orthogonally directed to the exciting electric current, suggesting MMF. In each of the components of magnetic field $\mathbf{H}$, (10) and (11) are respectively rewritten by (12) and (13)

$$\nabla^2 H = -\frac{Ni}{V} \quad \text{in static field} \tag{12}$$

$$\nabla^2 H - \sigma\mu \frac{dH}{\partial t} = -\frac{Ni}{V} \quad \text{in quasi-static field} \tag{13}$$

where N and $V(\mathrm{m}^3)$ denote the number of coil turns and volume concerned with MMF Ni, respectively. As in Fig. 2, the line electric current is equivalently represented by the positive and negative magnetic currents in the two-dimensional model. In the classical magnetic circuit theory, i.e., a lumped parameter representation, MMF is treated as a concentrated magnetic field source. Our formulation makes it possible to introduce the idea of MMF into distribution parameter system.

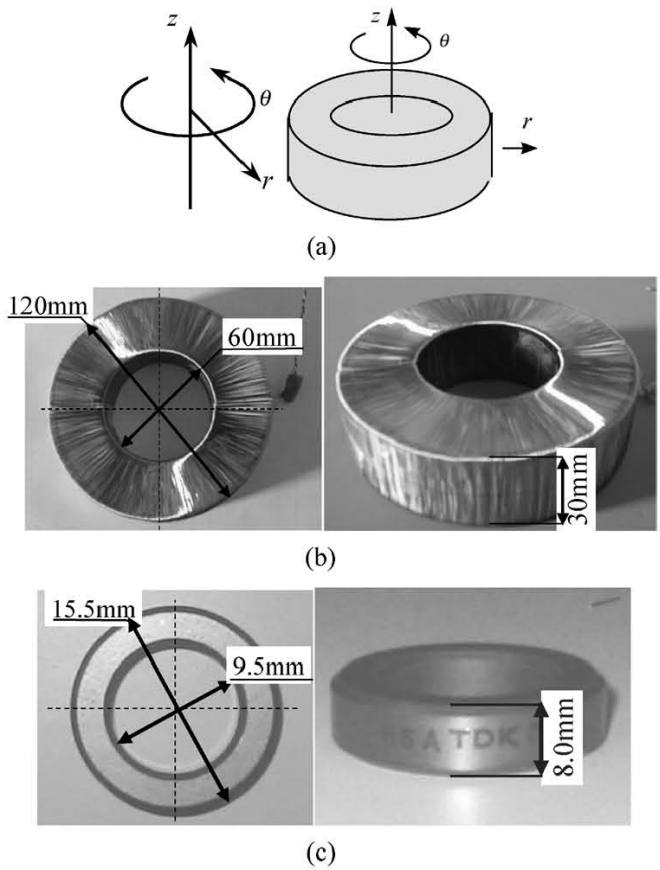

Fig. 3. Analysis models. (a) Definition of the problems. (b) Model A: Air-core coil (500 turns). (c) Model B: Magnetic-core (H5A ferrite core, TDK). Specification in each of models is listed in Table I.

III. Finite-Element Analyses

A. Models

To verify our formulation, we deal with axisymmetrical problems of the magnetic fields as illustrated in Fig. 3(a). Furthermore, we prepare the toroidal inductors of air-core [Model A: Fig. 3(b)] and magnetic-core [Model B: Fig. 3(c)] for experimental verification. Consider the magnetic currents as MMF, then these problems are reduced into the axisymmetrical models, even though the exciting electrical current has r and z components.

B. Unbounded Effects and Strategic Dual Image Method

These models are essentially accompanied with unbounded effects due to the exciting coils. In other words, the magnetic field continues being distributed infinitely far from the source points. Applying the strategic dual image (SDI) method to the hypothetical boundary solves the unbounded effects [8].

The principal idea of SDI is an image method in the analytical electromagnetic field calculation. Consider the image field sources outside of the hypothetical boundary in order to cancel the actual field sources inside of the hypothetical boundary. Then the boundary condition can be derived from the same nature as the image method [9]. The total of magnetic currents

TABLE I
SPECIFICATION OF ANALYZED MODELS

	Model A	Model B
Number of coil turns	500	85
Number of coil layers	1	1
Exciting electric current i (A)	75.3×10^{-3}	20×10^{-3}
Diameter of magnetic coil d (m)	0.4×10^{-3}	0.8×10^{-3}

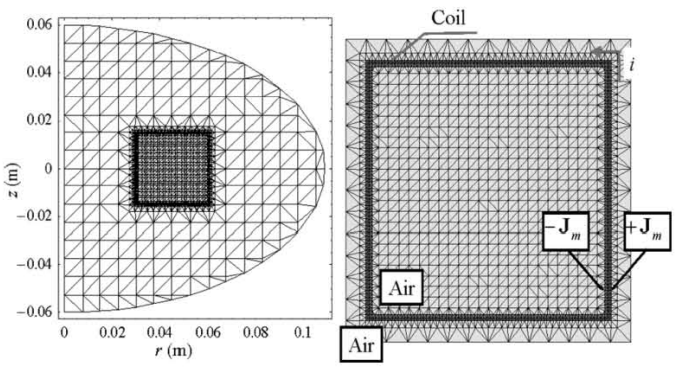

Fig. 4. Finite-element mesh system having elliptic shape for SDI method. The ratio of the major to minor axes is 1.815 : 1. The numbers of triangle elements and nodal points are 3626 and 1838, respectively. Left: entire mesh system. Right: Magnified elements in the vicinity of magnetic coil.

is zero as expressed in (8), so that the image magnetic currents must be zero as well. The condition satisfies this constraint is represented by

$$\sum_{p=1}^{q} \frac{Ni_p}{r_p} = 0 \tag{14}$$

where p and q refer to the source point and total number of the source points, respectively. This means that the total of field sources becomes zero at the origin both $r = 0$ and $z = 0$ in the cylindrical coordinate system.

The finite-element subdivision used in the analysis of Model A is illustrated in Fig. 4. In case of the axisymmetrical problems, the hypothetical boundary forms an elliptic shape whose axial ratio is 1.815. For further details, see [8] and [9].

C. Governing Equation

Since the magnetic current is the cause of magnetic field, then (10) is essentially reduced into

$$\nabla^2 H_\theta = -\sigma J_{m\theta} \tag{15}$$

where the subscript θ refers to θ component. As described in Section II-C, the term $-\sigma J_{m\theta}$ in (15) corresponds to MMF per volume. The volume is associated with magnetic coil volume having the area of S and the length as the flux path of $2\pi r$ where r is a distance from z axis, representing the pitch of coil winding

$$\nabla^2 H_\theta = -\frac{1}{S}\frac{Ni}{2\pi r}. \tag{16}$$

The finite-element discretization of (16) yields the system of equations with the manner of Fig. 2, It should be noted that the zero Dirichlet type boundary condition is obtained between $+J_{m\theta}$ and $-J_{m\theta}$ in Fig. 4.

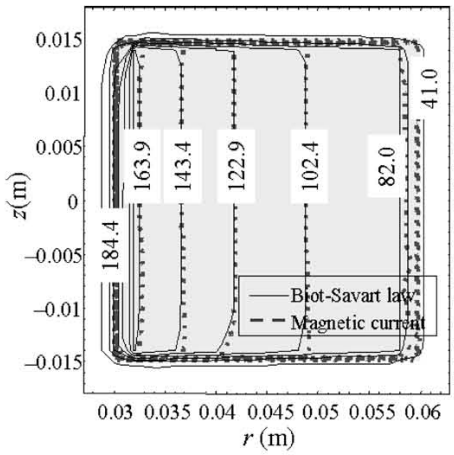

Fig. 5. Computed two-dimensional magnetic field distribution in the cross-sectional area of toroidal coil. The values on contours are in A/m. Comparison with computation based on Biot–Savart law is shown.

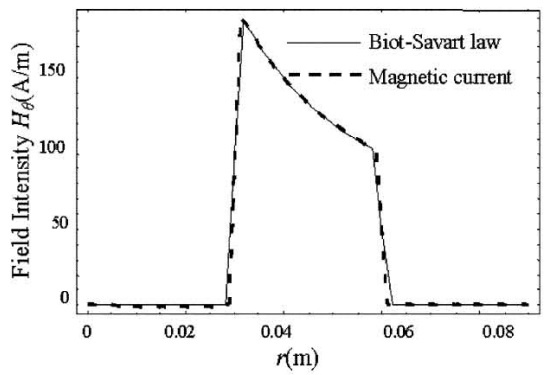

Fig. 6. Cross-sectional view along with $z = 0$ line in Fig. 5.

D. Model A

Fig. 5 shows the contour lines representation of computed magnetic field distribution for Model A. In Fig. 5, the solid and dotted contours show the analytical solution with Biot–Savart law and finite-element solution, respectively. Fig. 6 shows the cross-sectional view along with $z = 0$ line in Fig. 5. Both results well correspond each other. Fig. 7 shows an experimental result of magnetic field distribution of $z = 0$ line which is corresponding to those of Fig. 6. The experiment with the toroidal air-coil shown in Fig. 3(b) is carried out at an exciting frequency of 400 kHz. A pancake-type pickup coil sensor of 20 turns is used to measure the magnetic field as its induced voltages. Due to the large cross-sectional area $(8.7 \times 10^{-6}\ \mathrm{m}^2)$ of the sensor, the experimental result shown in Fig. 7 is normalized by the value at $r = 0.045$ (m). On the other hand, the measured inductance in Fig. 8 supports the finite-element solution whose inductance is 0.91 mH. Therefore, it suggests that the experimental result of Fig. 7 traces the computed result with good accuracy. Model A reveals that our formulation is capable of calculating magnetic field intensity accurately.

E. Model B

Model B in Fig. 3(c) demonstrates calculating hysteresis loops at 10 kHz. A Chua-type magnetization model is employed to represent relation between magnetic field H and flux

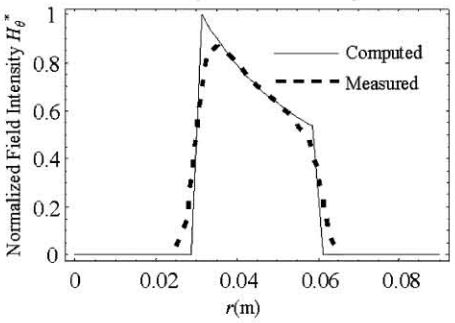

Fig. 7. Experimented magnetic field distribution on $z = 0$ line. *Normalized by the value at $r = 0.045$ (m).

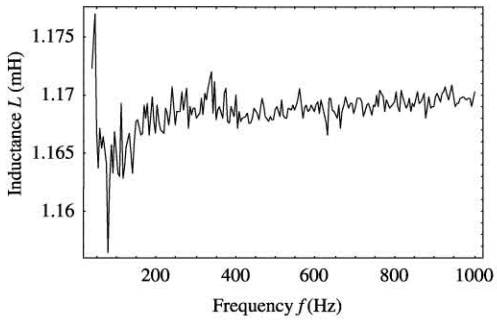

Fig. 8. Frequency characteristics of inductance for the tested toroidal air-core coil. Measurement device is HP4294A gain-phase impedance analyzer.

density B [10]–[12]. According to this magnetization model, a complex permeability $\mu(\omega)$ (H/m) in (17) can be applied under the high frequencies that both H and B are sinusoidal functions

$$\mu(\omega) = \frac{B}{H} = \left(1 + j\omega\frac{\mu_r}{s}\right)\left(\frac{1}{\mu} + j\omega\frac{1}{s}\right)^{-1} \qquad (17)$$

where μ, μ_r, and s denote permeability (H/m), reversible permeability (H/m), and hysteresis parameter (Ω/m), respectively; j and ω are complex number unit ($\sqrt{-1}$) and angular frequency (rad/s), respectively. Table II lists the measured linearized parameters used in this calculation.

Fig. 9 shows computed and measured hysteresis loops of H5A ferrite core inductor shown in Fig. 3(c). The computed result is obtained by averaging flux densities at the nodes on the core part, accurately reproducing the measured one. It is obvious that our formulation represents MMF in the modern computational methodologies in a quite efficient manner.

IV. Conclusion

We have succeeded in introducing the magnetic currents into magnetic field computation in terms of MMF. The magnetic currents have the orthogonal direction to the exciting electric current, so it takes MMF to the magnetic field computation methodologies. Since the relationship between MMF in the classical magnetic circuit theory and modern magnetic field computation methodologies has been clarified, then electrical circuit coupled problems can be efficiently addressed by our formulation.

TABLE II
Measured Parameters of Complex Permeability

Permeability μ (H/m)	6.68×10^{-3}
Reversible permeability μ_r (H/m)	1.55×10^{-4}
Hysteresis parameter s (Ω/m)	321.47

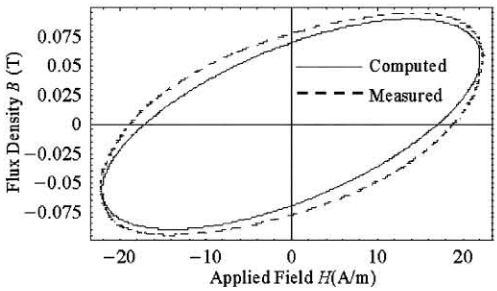

Fig. 9. Computed and measured hysteresis loops of H5A ferrite core inductor. Sinusoidal exciting voltage at a frequency of 10 kHz is applied.

Acknowledgment

This work was performed as a part of Grant-in-Aid for JSPS Fellows(16•2972) by the Ministry of Education, Culture, Sports, Science and Technology, Japan. The authors are grateful to T. Sato of Tohoku University for his help with experiments.

References

[1] K. Tajima, K. Sato, T. Komukai, and O. Ichinokura, "Reluctance network analysis of an orthogonal-core type parametric induction motor," *IEEE Trans. Magn.*, vol. 35, no. 5, pp. 3706–3708, Sep. 1999.

[2] P. Silvester, *Modern Electromagnetic Fields*. Englewood Cliffs, NJ: Prentice-Hall, 1968.

[3] P. Silvester and R. L. Ferrari, *Finite Elements for Electrical Engineers*. Cambridge, U.K.: Cambridge Univ. Press, 1983.

[4] Y. Saito, "Three-dimensional analysis of nonlinear magnetodynamic fields in a saturable reactor," *Comp. Meths. Appl. Mech. Eng.*, vol. 22, no. 3, Jun. 1980.

[5] R. F. Harrington, *Time-Harmonic Electromagnetic Fields*. New York: IEEE Press, 2001.

[6] J. Jin and J. L. Volakis, "A hybrid finite element method for scattering and radiation by microstrip patch antennas and arrays residing in a cavity," *IEEE Trans. Antennas Propagat.*, vol. 39, no. 11, pp. 1598–1604, Nov. 1991.

[7] J. A. Stratton, *Electromagnetic Theory*. New York: McGraw-Hill, 1941.

[8] Y. Saito, K. Takahashi, and S. Hayano, "Finite element solution of unbounded magnetic field problem containing ferromagnetic materials," *IEEE Trans. Magn.*, vol. 24, no. 6, pp. 2946–2948, Nov. 1988.

[9] K. Takahashi, S. Hayano, and Y. Saito, "The strategic dual image method for the open boundary electromagnetic field problems," *Int. J. Appl. Electromagn. Mater.*, vol. 4, no. 3, pp. 179–184, 1993.

[10] Y. Saito, S. Hayano, and N. Tsuya, "Experimental verification of a Chua type magnetization model," *IEEE Trans. Magn.*, vol. 25, no. 4, pp. 2968–2970, Jul. 1989.

[11] T. Naruta, H. Endo, S. Hayano, and Y. Saito, "A study of planar inductor," *Int. J. Appl. Electromagn. Mater.*, vol. 15, no. 1–4, pp. 403–408, 2001/2002.

[12] H. Endo, Y. Saito, S. Hayano, and K. Miya, "Classical and IT based magnetization dynamics modeling," *Int. J. Appl. Electromagn. Mech.*, vol. 16, no. 3–4, pp. 153–161, 2002.

Manuscript received June 8, 2004.